

## Study of the Charge Transfer Band Observed in Dialkoxo-Bridged Binuclear Copper(II) Complexes<sup>1)</sup>

Makoto HANDA,\* Tsutomu IDEHARA, Kenji NAKANO, Kuninobu KASUGA,  
Masahiro MIKURIYA,\*<sup>†</sup> Naohide MATSUMOTO,<sup>††</sup> Masahito KODERA,<sup>††</sup>  
and Sigeo KIDA\*,<sup>†††</sup>

Department of Chemistry, Faculty of Science, Shimane University,  
1060, Nishikawatsu, Matsue 690

<sup>†</sup>Department of Chemistry, School of Science, Kwansei Gakuin University,  
Uegahara, Nishinomiya 662

<sup>††</sup>Department of Chemistry, Faculty of Science, Kyushu University 33,  
Hakozaki, Higashiku, Fukuoka 812

<sup>†††</sup>Kumamoto Institute of Technology,

4-22, Ikeda, Kumamoto 860

(Received June 4, 1992)

The near-ultraviolet absorption band characteristic of dialkoxo-bridged binuclear copper(II) complexes was reinvestigated by using a series of binuclear copper(II) complexes with *N,N*-dialkyldiaminoalcohols,  $\text{Cu}_2\{\text{R}_2\text{N}(\text{CH}_2)_m\text{NH}(\text{CH}_2)_n\text{O}\}_2\text{X}'_2$  (abbreviated as  $\text{Cu}(\text{R}-m-n)\text{X}'$ ,  $\text{X}'=\text{ClO}_4, \text{BF}_4$ ). In this study eighteen complexes including ten new compounds were prepared and classified into two types, i.e., type-A and B according to Kida's classification, based on their temperature dependencies of magnetic susceptibilities (80–300 K) and reflectance spectra. The crystal structures of  $\text{Cu}(n\text{-Bu-3-2})\text{ClO}_4$  (**10**),  $\text{Cu}(\text{H-3-3})\text{BF}_4 \cdot \text{EtOH}$  (**11b**), and  $\text{Cu}(\text{Me-3-3})\text{ClO}_4$  (**12a**) were determined by the single-crystal X-ray diffraction method. The detailed analysis of the structures and reflectance spectra led to the same conclusion as Kida's one in assigning the near-ultraviolet absorption band. That is, the absorption was ascribed to the charge transfer (CT) from the bridging oxygen's nonbonding orbital to vacant copper d-orbital. On the other hand, in assigning the origin of the appearance of the CT band in the near-ultraviolet region, the conclusion different from Kida's one was presented. The origin was interpreted in terms of the red-shift of the band owing to the electrostatic repulsion between the bridging oxygen atoms. Moreover, the unusually low frequency and low intensity of the CT band of **12a** were also reasonably explained.

In the last three decades, a great number of dialkoxo-bridged binuclear copper(II) complexes have been prepared and extensive investigations of their structures and magnetic properties have revealed that the Cu–O–Cu bridge angle is the most important structural factor for the spin-exchange interaction between the copper(II) centers as had been shown in dihydroxo-bridged binuclear copper(II) complexes.<sup>2,3)</sup>

Another remarkable characteristic of the dialkoxo-bridged binuclear copper(II) complexes is a distinct absorption band appearing in the near-ultraviolet region. This is correlated with the magnetic property, and it is widely known that the both properties are most important factors for the characterization of the dialkoxo-bridged binuclear copper(II) complex.

Uhlig et al. prepared a number of copper(II) complexes with *N,N*-dialkylaminoalcohols,  $\text{Cu}(\text{R}_2\text{NCH}_2\text{CH}_2\text{O})\text{X}$  ( $\text{R}=\text{Me}, \text{Et}, n\text{-Bu}$  etc.;  $\text{X}=\text{Cl}, \text{Br}$ ) and classified into three groups on the basis of their electronic spectra and magnetic moments at room temperature.<sup>4)</sup>

Later, Nishida and Kida prepared a number of binuclear copper(II) complexes with *N,N*-dialkylaminoalcohols or *N,N*-dialkyldiaminoalcohols, and investigated the temperature dependencies of magnetic susceptibilities (80–300 K) and spectral properties of the complexes. They inspected in detail all the data together with already reported ones and classified the dialkoxo-bridged binuclear copper(II) complexes into following three types:<sup>5–10)</sup>

Type-A; the complexes of a dimer structure shown in Fig. 1. The magnetic moments are subnormal at room temperature and the  $\chi_A-T$  curves obey the Bleaney–Bowers equation. In the reflectance spectra the complexes show a distinct absorption band in the near-ultraviolet region ( $25\text{--}28 \times 10^3 \text{ cm}^{-1}$ ).

Type-B; the complexes of a cubane structure as shown in Fig. 2. Their magnetic moments are normal at room temperature and the  $\chi_A-T$  curves obey the Curie–Weiss law with a positive Weiss constant. In the reflectance spectra, the complexes show no distinct absorption band in the near-ultraviolet region.

Type-C; the complexes with a subnormal magnetic moment at room temperature, but the  $\chi_A-T$  curves do not obey the Bleaney–Bowers equation. They show only weak peaks as discernible shoulders in the near-ultraviolet region.

In other words, an antiferromagnetic interaction is operative when a distinct absorption band is observed in

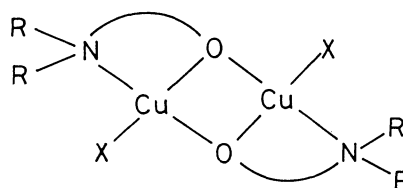


Fig. 1. Di- $\mu$ -(O,O')dihalogenobis(aminoalcoholato)-dicopper(II); type-A complex.

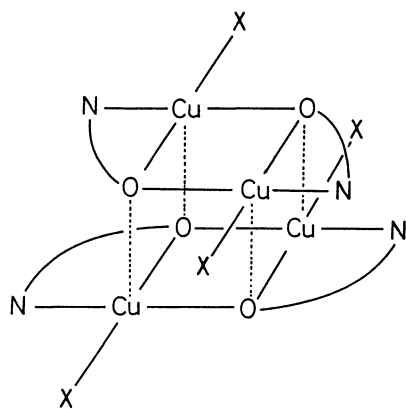


Fig. 2. Schematic illustration of the cubane type tetranuclear copper(II) complex.

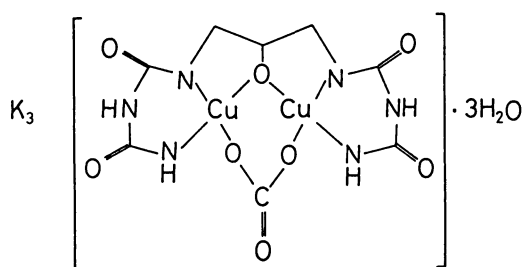


Fig. 3. Structure of  $K_3[Cu_2(bidl)(CO_3)] \cdot 3H_2O$ .

the near-ultraviolet region, whereas antiferromagnetic interaction is not operative for the complexes when there is no distinct absorption band in the near-ultraviolet region. They assigned the near-ultraviolet band to a charge transfer (CT) transition from the nonbonding orbital of the bridging oxygen to the vacant copper d-orbital. The emergence of the band in the near-ultraviolet region was explained as follows: "On forming the binuclear structure, the CT band which is originally located in a higher wavenumber region in the mononuclear state shifts to the near-ultraviolet region, because the energy of the nonbonding orbital is raised by a decrease of contribution of 2s-orbital to the nonbonding orbital owing to the increased planarity of three bonds linked to the bridging oxygen." This interpretation was applicable to most alkoxo-bridged binuclear copper(II) complexes and useful to understand the spectral properties of the complexes. Recently, however, some questions for the Nishida and Kida's interpretation have been presented. For example, a singly alkoxo-bridged binuclear copper(II) complex,  $K_3[Cu_2(bidl)(CO_3)] \cdot 3H_2O$  (Fig. 3) shows no distinct absorption band in the near-ultraviolet region in spite of a strong antiferromagnetic interaction within a molecule.<sup>11)</sup> A dialkoxo-bridged binuclear copper(II) complex,  $Cu_2\{(CH_3)_2N(CH_2)_3NH(CH_2)_3O\}_2(ClO_4)_2$  (numbered as **12a** in this report, see below) belonging to type-A shows a distinct absorption band at a much lower frequency ( $22.6 \times 10^3 \text{ cm}^{-1}$ )<sup>10)</sup> compared with those of the

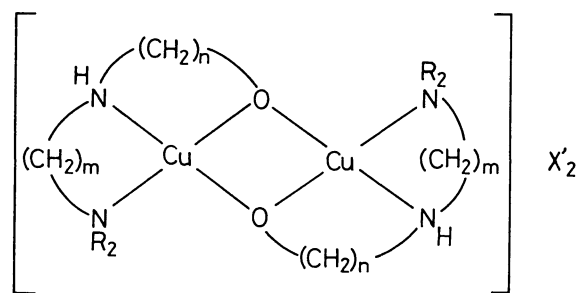


Fig. 4. Dialkoxo-bridged binuclear copper(II) complex  $Cu(R-m-n)X'$ , where  $(R-m-n)$  represents  $R_2N(CH_2)_mNH(CH_2)_nO$ .

Table 1. List of the Dialkoxo-Bridged Copper(II) Complexes

| No.        | $Cu(R-m-n)X' \cdot p(\text{solvent}) \cdot q(H_2O)$ |   |   |         |     |         |     |
|------------|---|---|---|---------|-----|---------|-----|
|            | R   | m | n | X'      | p   | solvent | q   |
| <b>1a</b>  | H   | 2 | 3 | $ClO_4$ | 1/2 | MeOH    | 0   |
| <b>1b</b>  | H   | 2 | 3 | $BF_4$  | 0   |         | 0   |
| <b>2</b>   | Me  | 2 | 3 | $ClO_4$ | 0   |         | 0   |
| <b>3a</b>  | Et  | 2 | 3 | $ClO_4$ | 0   |         | 0   |
| <b>3b</b>  | Et  | 2 | 3 | $BF_4$  | 1/2 | MeOH    | 0   |
| <b>4</b>   | <i>n</i> -Pr  | 2 | 3 | $ClO_4$ | 0   |         | 0   |
| <b>5</b>   | <i>n</i> -Bu  | 2 | 3 | $ClO_4$ | 0   |         | 0   |
| <b>6a</b>  | H   | 3 | 2 | $ClO_4$ | 1/8 | MeCN    | 0   |
| <b>6b</b>  | H   | 3 | 2 | $BF_4$  | 1/8 | MeCN    | 0   |
| <b>7a</b>  | Me  | 3 | 2 | $ClO_4$ | 1   | MeOH    | 0   |
| <b>7b</b>  | Me  | 3 | 2 | $BF_4$  | 1/2 | MeOH    | 1/2 |
| <b>8</b>   | Et  | 3 | 2 | $ClO_4$ | 0   |         | 0   |
| <b>9</b>   | <i>n</i> -Pr  | 3 | 2 | $ClO_4$ | 0   |         | 0   |
| <b>10</b>  | <i>n</i> -Bu  | 3 | 2 | $ClO_4$ | 0   |         | 0   |
| <b>11a</b> | H   | 3 | 3 | $ClO_4$ | 1   | MeOH    | 0   |
| <b>11b</b> | H   | 3 | 3 | $BF_4$  | 1   | EtOH    | 0   |
| <b>12a</b> | Me  | 3 | 3 | $ClO_4$ | 0   |         | 0   |
| <b>12b</b> | Me  | 3 | 3 | $BF_4$  | 0   |         | 0   |

corresponding band of the other type-A complexes ( $25-28 \times 10^3 \text{ cm}^{-1}$ ). Therefore, it is necessary to give a reasonable explanation to the unusual spectral features of the above complexes and to elucidate the correlation between the structure and magnetic and spectral properties for the whole alkoxo-bridged binuclear copper(II) complexes. Up to date, however, the study on spectral properties for the complexes is still limited.<sup>8,12)</sup>

In the present study, the origin of the near-ultraviolet band has been reinvestigated on the binuclear copper(II) complexes of *N,N*-dialkyldiaminoalcohols,  $Cu_2\{R_2N(CH_2)_mNH(CH_2)_nO\}_2X'_2 \cdot 2p(\text{solvent}) \cdot 2q(H_2O)$ ,  $X'=ClO_4, BF_4$  (they are represented as a general formula  $Cu(R-m-n)X' \cdot p(\text{solvent}) \cdot q(H_2O)$  as displayed in Fig. 4 and the numberings for the complexes are listed in Table 1). All these complexes are homologous with **12a** and were adopted for the following reasons.

(1) The ligands contain no double bond, and are terdentate so that no halide or pseudohalide ion is necessary to form a binuclear copper(II) complex different from the cases of bidentate aminoalcohols. Conse-

quently, the copper(II) complex has no absorption in the near-ultraviolet region due to intraligand or halogen-copper(II) charge transfer as observed for the complexes with aminoalcohols.

(2) The structures consisting of five and/or six membered chelate rings can be systematically varied by changing R or the number of methylene groups,  $m$  and  $n$  (Fig. 4).

### Experimental

**Preparations.** All the diamines and bromo- or chlorohydrins were obtained commercially except for  $N,N$ -di- $n$ -propylethylenediamine and  $N,N$ -di- $n$ -propyltrimethylenediamine which were prepared by a method similar to that of Banci et al.<sup>13)</sup>

The ligands  $R_2N(CH_2)_mNH(CH_2)_nOH$  ( $R=H$ , Me, Et,  $n$ -Pr,  $n$ -Bu;  $m=2$  or 3;  $n=2$  or 3) were prepared according to

the method of Keller et al.<sup>14)</sup> by the reaction of  $N,N$ -dialkylethylenediamine or  $N,N$ -dialkyltrimethylenediamine with ethylenechlorohydrin or trimethylenechlorohydrin. For the preparation of the ligand H( $n$ -Pr-2-3), trimethylenebromohydrin was used instead of trimethylenechlorohydrin because the latter did not react with the diamine.

The complexes were prepared by a method similar to that of Kida et al.<sup>10)</sup> To a warm solution of the ligand (6 mmol) and copper(II) perchlorate hexahydrate or copper(II) tetrafluoroborate hexahydrate (5 mmol) in 50 ml of absolute ethanol was added potassium  $t$ -butoxide (5 mmol). After refluxing for two hours, the solution was filtered and allowed to stand at room temperature. The crystals which separated were collected by filtration and recrystallized from an absolute methanol or ethanol solution. Recrystallization of **6a** and **6b** was made from acetonitrile. The results of elemental analyses for ten new complexes are summarized in Table 2.

**Measurements.** Carbon, hydrogen, and nitrogen analyses were carried out at the Service Center of Elemental Analysis of

Table 2. Elemental Analyses of the Complexes

| Complex   | Found/% |      |       | Calcd/% |      |       |
|---|---------|------|-------|---------|------|-------|
|   | C       | H    | N     | C       | H    | N     |
| Cu(H-2-3)BF <sub>4</sub> ( <b>1b</b> )                                | 22.30   | 4.86 | 10.36 | 22.45   | 4.90 | 10.47 |
| Cu(Et-2-3)BF <sub>4</sub> · ½ MeOH ( <b>3b</b> )                      | 33.42   | 6.83 | 8.29  | 33.59   | 6.83 | 8.25  |
| Cu( $n$ -Pr-2-3)ClO <sub>4</sub> ( <b>4</b> )                         | 36.03   | 7.17 | 7.43  | 36.26   | 6.92 | 7.69  |
| Cu( $n$ -Bu-2-3)ClO <sub>4</sub> ( <b>5</b> )                         | 39.79   | 7.48 | 7.02  | 39.79   | 7.45 | 7.14  |
| Cu(H-3-2)BF <sub>4</sub> · ½ MeCN ( <b>6b</b> )                       | 22.90   | 5.10 | 10.94 | 23.13   | 4.94 | 10.92 |
| Cu(Me-3-2)BF <sub>4</sub> · ½ MeOH · ½ H <sub>2</sub> O ( <b>7b</b> ) | 28.20   | 6.20 | 8.62  | 28.10   | 6.29 | 8.74  |
| Cu( $n$ -Pr-3-2)ClO <sub>4</sub> ( <b>9</b> )                         | 35.68   | 6.84 | 7.59  | 36.26   | 6.92 | 7.69  |
| Cu( $n$ -Bu-3-2)ClO <sub>4</sub> ( <b>10</b> )                        | 39.59   | 7.32 | 7.09  | 39.79   | 7.45 | 7.14  |
| Cu(H-3-3)BF <sub>4</sub> · EtOH ( <b>11b</b> )                        | 28.79   | 6.28 | 8.64  | 29.33   | 6.46 | 8.55  |
| Cu(Me-3-3)BF <sub>4</sub> ( <b>12b</b> )                              | 30.71   | 6.10 | 8.81  | 31.04   | 6.19 | 9.05  |

Table 3. Crystal Data and Data Collection Details for **10**, **11b**, and **12a**

|  | <b>10</b>  | <b>11b</b>  | <b>12a</b>   |
|--|--|---|--|
| Formula                                  | C <sub>26</sub> H <sub>58</sub> Cl <sub>2</sub> Cu <sub>2</sub> N <sub>4</sub> O <sub>10</sub> | C <sub>16</sub> H <sub>42</sub> B <sub>2</sub> F <sub>8</sub> Cu <sub>2</sub> N <sub>4</sub> O <sub>4</sub> | C <sub>16</sub> H <sub>38</sub> Cl <sub>2</sub> Cu <sub>2</sub> N <sub>4</sub> O <sub>10</sub> |
| $M$                                      | 784.76   | 655.23  | 644.50   |
| Crystal system                           | Triclinic  | Monoclinic  | Monoclinic   |
| Space group                              | $P\bar{1}$   | $P2_1/a$  | $P2_1/a$   |
| $a/\text{\AA}$                           | 9.829(3)   | 16.004(2)   | 16.435(4)  |
| $b/\text{\AA}$                           | 12.431(3)  | 9.579(2)  | 14.522(3)  |
| $c/\text{\AA}$                           | 8.741(3)   | 9.410(1)  | 11.678(2)  |
| $\alpha/^\circ$                          | 104.15(2)  | 90  | 90   |
| $\beta/^\circ$                           | 115.77(2)  | 103.16(1)   | 109.98(2)  |
| $\gamma/^\circ$                          | 69.53(2)   | 90  | 90   |
| $U/\text{\AA}^3$                         | 895.6  | 1404.7  | 2619.4   |
| $Z$                                      | 1  | 2   | 4  |
| $D_c/\text{g cm}^{-3}$                   | 1.45   | 1.55  | 1.63   |
| $D_m/\text{g cm}^{-3}$                   | 1.43   | 1.54  | 1.62   |
| Crystal size/mm                          | 0.2×0.2×0.2  | 0.3×0.3×0.4   | 0.2×0.2×0.4  |
| $\mu(\text{Mo } K\alpha)/\text{cm}^{-1}$ | 13.9   | 16.0  | 18.9   |
| Scan speed/ $^\circ \text{ min}^{-1}$    | 4  | 4   | 2  |
| $2\theta_{\text{max}}/^\circ$            | 52   | 46  | 46   |
| No. of reflections measured              | 3368   | 1184  | 4136   |
| No. of unique reflections                | 3197   | 944   | 2632   |
| $[F_o > 3\sigma(F_o)]$                   |  |   |  |
| Weighting scheme ( $w=$ )                | $1/\sigma^2(F_o)$  | $1/\sigma^2(F_o)$   | $[\sigma^2 + (0.015 F_o )^2]^{-1}$   |
| $R^{\text{a)}}$                          | 4.04   | 8.34  | 5.50   |
| $R'^{\text{b)}}$                         | 3.55   | 4.66  | 5.50   |

a)  $\sum ||F_o| - |F_c|| / \sum |F_o|$ . b)  $[\sum w(|F_o| - |F_c|)^2 / \sum w|F_o|^2]^{1/2}$ .

Table 4. Atomic Coordinates ( $\times 10^4$ ) and Thermal Parameters

| Atom       | <i>x</i> | <i>y</i>  | <i>z</i> | <i>B</i> <sub>eq</sub> /Å <sup>2</sup> | Atom       | <i>x</i> | <i>y</i>  | <i>z</i> | <i>B</i> <sub>eq</sub> /Å <sup>2</sup> |
|------------|----------|-----------|----------|--|------------|----------|-----------|----------|--|
| <b>10</b>  |          |           |          |  |            |          |           |          |  |
| Cu         | 228(0)   | 1165(0)   | 878(1)   | 2.3                                    | F2         | 3019(6)  | −3683(11) | 1087(12) | 12.4                                   |
| O1         | 1415(2)  | −412(2)   | 551(3)   | 2.9                                    | F3         | 2327(7)  | −5578(11) | 1049(11) | 13.7                                   |
| N1         | 2291(3)  | 1506(2)   | 1659(4)  | 2.9                                    | F4         | 3310(7)  | −5071(15) | 2889(13) | 17.1                                   |
| N2         | −1049(3) | 2774(2)   | 1355(3)  | 2.6                                    | <b>12a</b> |          |           |          |  |
| C1         | 3033(4)  | −568(3)   | 981(5)   | 3.5                                    | Cu1        | 7987(1)  | 4177(1)   | 9089(1)  | 2.3                                    |
| C2         | 3493(4)  | 418(3)    | 2278(5)  | 3.7                                    | Cu2        | 8785(1)  | 3473(1)   | 7362(1)  | 2.2                                    |
| C3         | 2647(4)  | 2516(3)   | 2852(5)  | 3.5                                    | Cl1        | 8778(1)  | 6165(1)   | 11440(2) | 3.4                                    |
| C4         | 1284(4)  | 3589(3)   | 2373(5)  | 3.5                                    | Cl2        | 8891(1)  | −1245(2)  | 6191(2)  | 4.4                                    |
| C5         | −124(4)  | 3561(3)   | 2649(4)  | 3.1                                    | O1         | 8766(3)  | 3201(3)   | 8986(4)  | 2.5                                    |
| C6         | −1868(4) | 3206(3)   | −390(4)  | 2.9                                    | O2         | 8322(3)  | 4615(3)   | 7751(4)  | 2.5                                    |
| C7         | −2943(5) | 4431(3)   | −472(5)  | 4.1                                    | O3         | 9576(4)  | 6644(5)   | 11941(5) | 5.0                                    |
| C8         | −3878(5) | 4713(3)   | −2317(5) | 4.1                                    | O4         | 8842(4)  | 5483(4)   | 10594(5) | 5.0                                    |
| C9         | −5133(5) | 4104(3)   | −3329(5) | 4.7                                    | O5         | 8594(5)  | 5704(5)   | 12414(6) | 7.1                                    |
| C10        | −2217(4) | 2731(3)   | 1990(4)  | 3.0                                    | O6         | 8114(5)  | 6785(5)   | 10895(8) | 9.0                                    |
| C11        | −1522(4) | 1881(3)   | 3305(4)  | 3.4                                    | O7         | 9419(6)  | −768(6)   | 7191(8)  | 10.3                                   |
| C12        | −2721(5) | 1950(3)   | 3992(5)  | 5.0                                    | O8         | 8214(5)  | −734(6)   | 5466(8)  | 10.8                                   |
| C13        | −2153(5) | 1094(4)   | 5232(6)  | 5.6                                    | O9         | 9325(7)  | −1720(10) | 5579(9)  | 14.6                                   |
| Cl         | 2375(1)  | 2353(1)   | −2129(1) | 4.6                                    | O10        | 8508(7)  | −1971(7)  | 6673(9)  | 11.6                                   |
| O2         | 3570(4)  | 2572(3)   | −560(4)  | 8.4                                    | N1         | 7842(4)  | 3505(4)   | 10513(5) | 3.0                                    |
| O3         | 2914(5)  | 1804(3)   | −3425(4) | 9.7                                    | N2         | 6802(4)  | 4801(4)   | 8463(5)  | 2.6                                    |
| O4         | 1626(6)  | 1660(4)   | −1954(5) | 12.5                                   | N3         | 8750(4)  | 4006(4)   | 5756(5)  | 2.6                                    |
| O5         | 1238(5)  | 3377(3)   | −2625(6) | 14.3                                   | N4         | 8631(4)  | 2113(4)   | 6828(6)  | 2.9                                    |
| <b>11b</b> |          |           |          |  |            |          |           |          |  |
| Cu         | 846(1)   | 265(2)    | 1090(2)  | 4.2                                    | C1         | 9517(5)  | 3069(6)   | 10017(7) | 3.2                                    |
| O1         | −242(5)  | 1100(9)   | 281(10)  | 4.8                                    | C2         | 9275(5)  | 2686(6)   | 11042(7) | 3.5                                    |
| N1         | 1959(6)  | −789(11)  | 1527(12) | 5.3                                    | C3         | 8694(6)  | 3303(6)   | 11474(7) | 3.6                                    |
| N2         | 1411(7)  | 1950(12)  | 2165(13) | 5.8                                    | C4         | 7230(6)  | 3870(7)   | 11086(7) | 4.1                                    |
| C1         | 2518(9)  | −641(16)  | 2905(18) | 8.7                                    | C5         | 6351(6)  | 4108(7)   | 10154(8) | 4.3                                    |
| C2         | 2742(8)  | 820(17)   | 3241(19) | 9.7                                    | C6         | 6370(5)  | 4920(6)   | 9394(8)  | 3.9                                    |
| C3         | 2071(11) | 1690(17)  | 3481(16) | 9.5                                    | C7         | 6815(6)  | 5709(6)   | 7900(8)  | 4.0                                    |
| C4         | 773(11)  | 2969(17)  | 2512(18) | 9.0                                    | C8         | 6288(5)  | 4161(6)   | 7499(7)  | 4.0                                    |
| C5         | 163(10)  | 3397(14)  | 1265(18) | 9.5                                    | C9         | 8780(5)  | 5446(5)   | 7721(7)  | 2.9                                    |
| C6         | −531(9)  | 2398(15)  | 670(17)  | 7.4                                    | C10        | 8685(6)  | 5636(6)   | 6403(7)  | 3.6                                    |
| O2         | 232(6)   | −562(11)  | 3095(10) | 7.4                                    | C11        | 9128(6)  | 4951(6)   | 5843(7)  | 3.4                                    |
| C7         | 278(12)  | −1645(19) | 4084(18) | 11.2                                   | C12        | 9139(6)  | 3432(6)   | 5007(7)  | 3.8                                    |
| C8         | 105(10)  | −2927(19) | 3548(19) | 10.1                                   | C13        | 8750(6)  | 2476(6)   | 4762(8)  | 4.0                                    |
| B          | 2684(12) | −4546(20) | 1912(20) | 7.3                                    | C14        | 8994(6)  | 1850(6)   | 5856(8)  | 3.8                                    |
| F1         | 2172(6)  | −3922(10) | 2603(12) | 10.7                                   | C15        | 7682(6)  | 1999(6)   | 6382(8)  | 4.1                                    |
|            |          |           |          |  | C16        | 9015(7)  | 1470(6)   | 7857(8)  | 4.6                                    |

Kyushu University. Diffuse reflectance spectra were measured with a Shimadzu multipurpose spectrophotometer MPS-2000 at room temperature. Magnetic susceptibilities in the range from liquid nitrogen to room temperature were determined by the Faraday method. The apparatus was calibrated by the use of  $[\text{Ni}(\text{en})_3]\text{S}_2\text{O}_3$  ( $\text{en}$ =ethylenediamine),<sup>15)</sup> and diamagnetic corrections were made by the use of Pascal's constants. Effective magnetic moments were calculated from the equation,  $\mu_{\text{eff}} = 2.828(\chi_A \cdot T)^{1/2}$ , where  $\chi_A$  is the magnetic susceptibility per a copper atom.

**X-Ray Diffraction Analyses.** Diffraction data were measured on a Rigaku AFC-5 automated four-circle diffractometer with graphite monochromatized Mo  $K\alpha$  radiation at  $293 \pm 1$  K. Pertinent crystallographic parameters are summarized in Table 3. The intensity data were collected by the  $\theta$ – $2\theta$  scan technique. For **10** and **12a**, three standard reflections were monitored every 100 reflections. The intensities showed a good stability. In the case of **11b**, the crystal readily effloresced in the atmosphere, hence it was enclosed in a glass capillary saturated with ethanol vapor. Two standard reflections were monitored every 100 reflections. No significant decay of the intensities was observed during the data collec-

tion. The intensity data of each complex were corrected for the Lorentz-polarization effects but not for absorption.

The structure was solved by the heavy-atom method for **10** and **11b** and by the direct method for **12a**. Refinement was carried out by the block-diagonal least-squares method. Atomic scattering factors were taken from Ref. 16. Anisotropic thermal parameters were adopted for non-hydrogen atoms. The hydrogen atoms of **10** were placed in calculated positions with isotropic thermal parameters and refined in the last cycle of the block-diagonal least-square calculation. For **11b** and **12a**, the hydrogen atoms were inserted in their calculated positions and included in the structure-factor calculations, but their parameters were not refined.

Above calculations were carried out on a FACOM-M 780 computer at the Computer Center of Kyushu University for **10** and **11b** and on a HITAC M-680H computer at the Computer Center of the Institute for Molecular Science for **12a** by the use of the UNICS III,<sup>17,18)</sup> MULTAN 78,<sup>19)</sup> and ORTEP programs.<sup>20)</sup> Atomic coordinates and thermal parameters of non-hydrogen atoms are listed in Table 4. The anisotropic thermal parameters of non-hydrogen atoms, the atomic coordinates and thermal parameters of hydrogen atoms, and

$F_o$ – $F_c$  tables have been deposited as a Document No. 9045 at the Office of the Editor of Bull. Chem. Soc. Jpn.

## Results

**Description of the Structures.** Perspective drawings of the binuclear cation units of **10**, **11b**, and **12a** are shown in Figs. 5, 6, and 7, respectively. The crystals of all three compounds consist of dialkoxo-bridged binuclear cation units and their counter anions,  $\text{BF}_4^-$  or  $\text{ClO}_4^-$ .

**10** has a centrosymmetry at the center of the cation molecule, hence the Cu, Cu<sup>i</sup>, O1, O1<sup>i</sup> atoms are located on the same plane. Each copper ion adopts an essentially planar configuration with the amino nitrogens N1, N2 and bridging oxygens O1, O1<sup>i</sup>. The deviation from the plane formed by N1, N2, O1, and O1<sup>i</sup> is only 0.09 Å. The perchlorate ion is far apart from the cation (>3.5 Å), and does not participate in coordination.

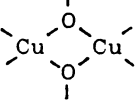
**11b** also has a centrosymmetry and the coordination geometry is essentially square pyramidal in which the apical site is occupied by the oxygen atom of ethanol with the distance of 2.448(11) Å. The deviation of Cu from the basal plane is 0.14 Å toward the apical site. The tetrafluoroborate ion does not participate in coordination. The shortest distance between Cu and F ( $\text{BF}_4^-$ ) is 3.194(12) Å.

In the case of **12a**, two crystallographically independent perchlorate ions exist in the crystal and one of them (designated as C11, O3, O4, O5, and O6) is weakly coordinated to the copper atoms with the interatomic

distances of Cu1–O4 and Cu2–O3<sup>i</sup>, 2.641(6) and 2.539(6) Å, respectively. The coordination geometry of each copper atom is an elongated square pyramid with a perchlorate oxygen at the apex. The copper ions Cu1 and Cu2 are displaced by 0.26 and 0.25 Å, respectively, from the basal plane toward the perchlorate oxygen.

In Table 5, some structural parameters of **10**, **11b**, and **12a** are listed together with those of **3a** and **7a** already reported.<sup>21,22)</sup> As for the Cu–Cu, Cu–O, Cu–N, and O–O distances, no remarkable difference can be found in the complexes and their values are common for the corresponding distances of dialkoxo-bridged binuclear copper(II) complexes so far reported.<sup>2)</sup>

The most noticeable point for **3a** and **12a** is that the

 bridging system is considerably bent, i.e., dihedral angles ( $D$ ) between  $\text{CuO}_2$  planes sharing the O–O edge is 164.7° (**3a**) and 158.2° (**12a**), which cer-

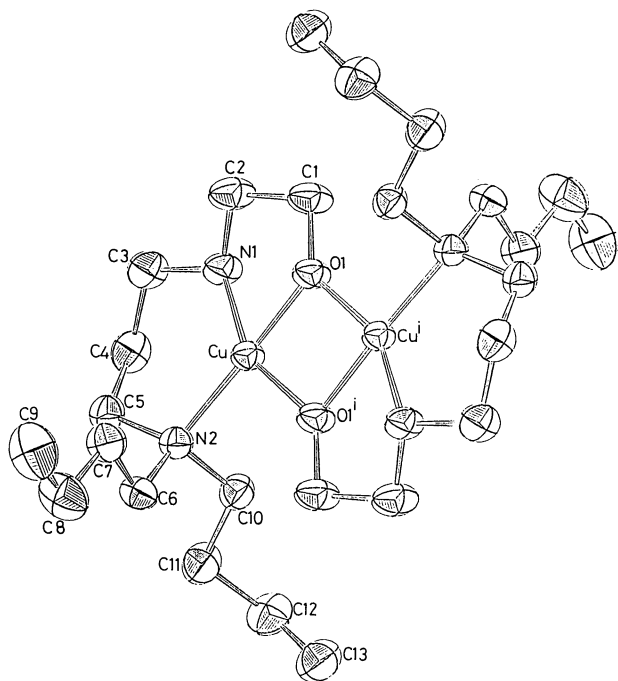


Fig. 5. A perspective view of binuclear cation unit of  $\text{Cu}(n\text{-Bu-3-2})\text{ClO}_4$  (**10**), where  $\text{ClO}_4^-$  are omitted for clarity. Superscript (i) refers to the equivalent position ( $-x, -y, -z$ ).

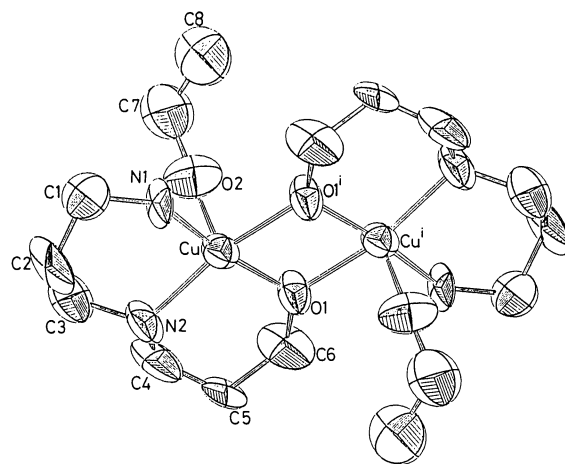


Fig. 6. A perspective view of binuclear cation unit of  $\text{Cu}(\text{H-3-3})\text{BF}_4$  (**11b**), where  $\text{BF}_4^-$  are omitted. Superscript (i) refers to the equivalent position ( $-x, -y, -z$ ).

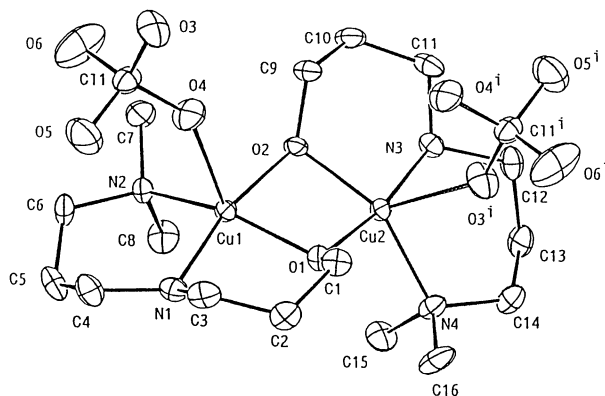


Fig. 7. A perspective view of binuclear cation unit of  $\text{Cu}(\text{Me-3-3})\text{ClO}_4$  (**12a**). Superscript (i) refers to the equivalent position ( $2-x, 1-y, 2-z$ ).

Table 5. Structural Parameters of the Complexes

| Complex    | Cu·Cu<br>Å | Cu-O<br>Å           | Cu-N<br>Å           | O·O<br>Å | Cu-axial<br>Å       | Cu-O-Cu<br>°       | $D^b)$<br>° | $\rho^c)$<br>°    | $d_c^d)$<br>Å      | Ref.      |
|------------|------------|---------------------|---------------------|----------|---------------------|--------------------|-------------|-------------------|--------------------|-----------|
| <b>3a</b>  | 2.953      | 1.935 <sup>a)</sup> | 2.027 <sup>a)</sup> | 2.47     | 2.57 <sup>a)</sup>  | 99.4 <sup>a)</sup> | 164.7       | 352 <sup>a)</sup> | 0.55 <sup>a)</sup> | 21        |
| <b>7a</b>  | 3.034      | 1.930 <sup>a)</sup> | 2.031 <sup>a)</sup> | 2.39     | 2.348               | 103.6              | 180         | 355               | 0.46               | 22        |
| <b>10</b>  | 3.013      | 1.934 <sup>a)</sup> | 2.008 <sup>a)</sup> | 2.42     |                     | 102.4              | 180         | 357               | 0.34               | This work |
| <b>11b</b> | 3.045      | 1.922 <sup>a)</sup> | 2.008 <sup>a)</sup> | 2.35     | 2.448               | 104.8              | 180         | 360               | 0.05               | This work |
| <b>12a</b> | 2.939      | 1.941 <sup>a)</sup> | 2.032 <sup>a)</sup> | 2.47     | 2.590 <sup>a)</sup> | 98.4 <sup>a)</sup> | 158.2       | 341 <sup>a)</sup> | 0.86 <sup>a)</sup> | This work |

a) Mean value. b) Dihedral angle between the two CuO<sub>2</sub> planes. c) Sum of the angles around the bridging oxygen atom. d) Deviation of the carbon atom linked to the oxygen atom from the Cu<sub>2</sub>O plane.

Table 6. Reflectance Spectral and Magnetic Data of the Complexes

| Complex    | Type | $\tilde{\nu}_{\max}/10^3 \text{ cm}^{-1}$ | $\mu_{\text{eff}}/\text{BM}^a)$ | $-2J/\text{cm}^{-1}$      | $g$               | $10^6 N\alpha/\text{cm}^3 \text{ mol}^{-1}$ | $P$              |
|------------|------|---|---------------------------------|---------------------------|-------------------|---|------------------|
| <b>1a</b>  | A    | 17.3                                      | 28.2                            | 0.65 <sup>b)</sup>        | 700 <sup>b)</sup> | 2.10 <sup>b)</sup>                          | 70 <sup>b)</sup> |
| <b>1b</b>  | A    | 17.8                                      | 27.6                            | 1.30                      | 310               | 2.01  | 30               |
| <b>2</b>   | A    | 16.5                                      | 25.8                            | 0.93 <sup>b)</sup>        | 530 <sup>b)</sup> | 2.08 <sup>b)</sup>                          | 60 <sup>b)</sup> |
| <b>3a</b>  | A    | 16.5                                      | 25.8                            | 0.93 <sup>b)</sup>        | 530 <sup>b)</sup> | 2.08 <sup>b)</sup>                          | 35 <sup>b)</sup> |
| <b>3b</b>  | A    | 16.2                                      | 25.8                            | 0.86                      | 610               | 2.08  | 30               |
| <b>4</b>   | A    | 17.2                                      | 26.2                            | 0.54                      | 850               | 2.06  | 30               |
| <b>5</b>   | A    | 16.8                                      | 26.7                            | 0.63                      | 740               | 2.02  | 15               |
| <b>7a</b>  | A    | 15.4                                      | 27.0                            | 1.11 <sup>c)</sup>        |                   |   |                  |
| <b>7b</b>  | A    | 15.4                                      | 27.3                            | 1.36                      | 310               | 2.02  | 30               |
| <b>8</b>   | A    | 15.7                                      | 26.5                            | 1.17                      | 430               | 2.10  | 100              |
| <b>9</b>   | A    | 16.3                                      | 26.1                            | 1.20                      | 400               | 2.06  | 60               |
| <b>10</b>  | A    | 17.0                                      | 25.8                            | 1.15                      | 430               | 2.08  | 60               |
| <b>11a</b> | A    | 17.2                                      | 27.8                            | 0.49                      | 860               | 2.01  | 10               |
| <b>11b</b> | A    | 17.3                                      | 27.8                            | 0.50                      | 860               | 2.05  | 15               |
| <b>12a</b> | A    | 16.9                                      | 22.6                            | 1.10                      | 460               | 2.06  | 60               |
| <b>12b</b> | A    | 17.2                                      | 22.9                            | 1.15                      | 390               | 2.03  | 30               |
| <b>6a</b>  | B    | 16.4                                      | 1.82                            | $(\theta=23.7 \text{ K})$ |                   |   |                  |
| <b>6b</b>  | B    | 16.8                                      | 1.92                            | $(\theta=27.1 \text{ K})$ |                   |   |                  |

a) At room temperature. b) Data from Ref. 10. c) Data from Ref. 22.

tainly links to the fact giving rise to relatively small Cu-O-Cu angles, 99.4° and 98.4°, respectively. Such a bent structure has been reported for some other dialkoxo-bridged binuclear copper(II) complexes, and **12a** has the second smallest dihedral angle in these homologous complexes.<sup>23)</sup>

It is also shown that the deviation from the planarity around the bridging oxygen atom of **12a** is extremely large. The non-planarity can be defined by the deviation ( $d_c$ ) of the carbon atom linked to the oxygen atom from the Cu-O-Cu plane or the sum ( $\rho$ ) of the three bond angles around the bridging oxygen atom. **12a** has the largest  $d_c$  value (0.86 Å) and smallest  $\rho$  one (341°) so that the geometry around the bridging oxygen atom considerably deviates from the planar arrangement.

**Spectral and Magnetic Properties.** The reflectance spectral and magnetic data of the eighteen copper(II) complexes with *N,N*-dialkyldiaminoalcohols prepared in this study are summarized in Table 6. The temperature dependencies of magnetic susceptibilities for these complexes were simulated by the modified Bleaney-Bowers equation including a correction term for paramagnetic impurities,

$$\chi_A = (Ng^2\beta^2/kT)[3 + \exp(-2J/kT)]^{-1}(1-P) + 0.45P/T + N\alpha, \quad (1)$$

where  $\chi_A$  is a susceptibility per copper atom,  $P$  is the fraction of the monomeric copper(II) impurity and other symbols have the usual meanings. The complexes except for **6a** and **6b** show a distinct band in the near-ultraviolet region (22.6–28.2×10<sup>3</sup> cm<sup>-1</sup>) in addition to a d-d absorption band (15–18×10<sup>3</sup> cm<sup>-1</sup>) and a strong spin-exchange coupling in their molecules ( $\mu_{\text{eff.}}$ =0.49–1.36 BM,  $-2J$ =310–860 cm<sup>-1</sup>). Thus, according to Nishida and Kida's classification the complexes should belong to type-A. On the other hand, **6a** and **6b** do not show such a distinct band in the near-ultraviolet region and their magnetic moments fall in the range of those of common mononuclear copper(II) complexes ( $\mu_{\text{eff.}}$ =1.82 BM (**6a**) and 1.92 BM (**6b**)). Thus, these complexes should belong to type-B.

## Discussion

As shown in Table 6, all the type-A complexes exhibit a strong antiferromagnetic spin-exchange interaction between copper ions and show a distinct absorption band in the near-ultraviolet region (22.6–28.2×10<sup>3</sup>

$\text{cm}^{-1}$ ). However, the complexes **12a** and **12b** display a strange behavior. According to Nishida and Kida's interpretation, the larger antiferromagnetic interaction, the larger red-shift of the CT band emerges. The wavenumbers of the absorption maxima of the CT bands of **12a** and **12b** are much lower than those expected from their  $-2J$  values ( $460\text{ cm}^{-1}$  (**12a**) and  $390\text{ cm}^{-1}$  (**12b**)). For example, **8** has a comparable  $-2J$  value ( $430\text{ cm}^{-1}$ ) with those of **12a** and **12b** but shows the absorption at  $26.5 \times 10^3\text{ cm}^{-1}$ ; **11a** and **11b** have much stronger antiferromagnetic interaction ( $860\text{ cm}^{-1}$ ) than **12a** and **12b** and show the band maxima at  $27.8 \times 10^3\text{ cm}^{-1}$ .

Moreover, it has been realized that the  $-2J$  value ( $460\text{ cm}^{-1}$ ) for **12a** is much larger than that expected from  $\angle\text{Cu-O-Cu}=98.4^\circ$ .<sup>2,3)</sup> In the previous report based on the theoretical calculation,<sup>3c)</sup> we pointed out that the decrease of the dihedral angle ( $D$ ) between two coordination plane from  $180^\circ$  leads to the increase of the magnetic interaction, though the Cu-O-Cu angle is surely the main structural factor to determine the  $J$  value. The dihedral angle ( $D$ ) of **12a** is  $158.2^\circ$ , which may give rise to a larger  $-2J$  value than that expected from its Cu-O-Cu bridge angle.

In Fig. 8,  $\tilde{\nu}_{\text{CT}}$ , the wavenumber of absorption maximum for the CT band, is plotted against  $\rho$ , parameter for the planarity around the bridging oxygen atom (cf. Table 5). The result indicates that the absorption maximum tends to shift to lower frequency as  $\rho$  decreases. This trend is in conflict with that predicted by Nishida and Kida's concept. According to their concept, the deviation from the planarity around the bridging oxygen should lead to the blue-shift of the CT band.

From the above discussions, in order to establish the comprehensive interpretation of the CT band the following two points should be settled.

(i) Why does the CT band generally appear in the near-ultraviolet region,  $25\text{--}28 \times 10^3\text{ cm}^{-1}$  in type-A complexes?

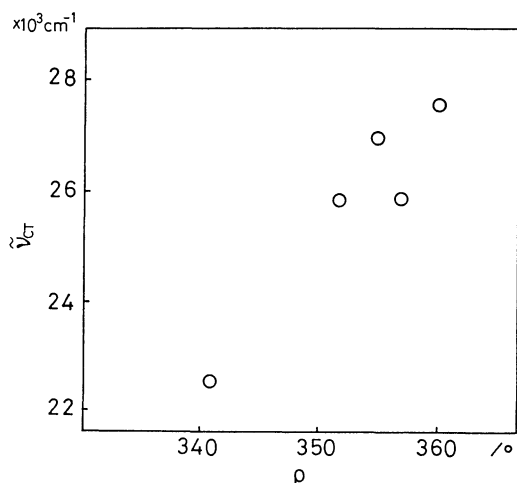


Fig. 8. Correlation between  $\tilde{\nu}_{\text{CT}}$ , CT wave number, and  $\rho$ , sum of the angles around the bridging oxygen atom.

(ii) Why do the CT bands of the complexes **12a** and **12b** appear at a significantly lower frequency region (ca.  $23 \times 10^3\text{ cm}^{-1}$ )?

As for question (i), it is first necessary to reconsider the origin of the band characteristic of dialkoxo-bridged binuclear copper(II) complexes. As shown in Table 6, the band maxima of the near-ultraviolet bands of all the complexes appear at a wavenumber higher than  $22.6 \times 10^3\text{ cm}^{-1}$ . The coordination geometries around copper ions of the type-A complexes are square or square pyramidal (cf. Figs. 5–7) and such copper(II) complexes generally exhibit d-d transition bands in the visible region with a molar extinction coefficient lower than ca.  $100\text{ mol}^{-1}\text{ dm}^3\text{ cm}^{-1}$ .<sup>24)</sup> Therefore, it is clear that the near-ultraviolet absorption is not a d-d transition band. Since the ligands have no absorption in the visible and near-ultraviolet region, there is no doubt that the band should be due to the CT transition from the nonbonding orbital of the bridging oxygen to the empty copper d-orbital. This assignment is also supported by the fact that the cubane type tetranuclear complexes shown in Fig. 2, which have no nonbonding orbital on the bridging oxygen, show no such distinct band in the near-ultraviolet region.<sup>5,6,10)</sup>

Moreover, monomeric alkoxo copper(II) complexes,  $[\text{Cu}(\text{eta})(\text{Heta})]_2(\text{NO}_3)_2$  ( $\text{Heta}=2\text{-aminoethanol}$ ) (**13**) (Fig. 9) and its derivative  $[\text{Cu}(\text{mep})(\text{Hmep})(\text{H}_2\text{O})]_2(\text{NO}_3)_2$  ( $\text{Hmep}=2\text{-amino-2-methylpropanol}$ ) (**14**) with Cu-O...H...O-Cu bridgings,<sup>25)</sup> and a hetero-metal complex  $\text{BaCu}(\text{maae}) \cdot 7\text{H}_2\text{O}$  ( $\text{H}_4\text{maae}=N,N'\text{-bis}(2\text{-hydroxy-})$

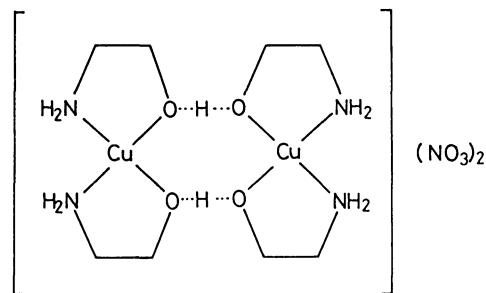


Fig. 9. Structure of  $[\text{Cu}(\text{eta})(\text{Heta})]_2(\text{NO}_3)_2$  (**13**). Two *cis*-bis(2-aminoethanolato)copper(II) complexes are joined by two hydrogen bonds to form the dimer structure.

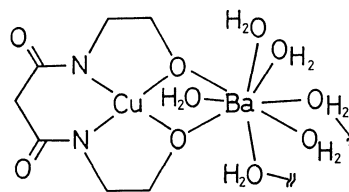
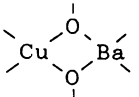
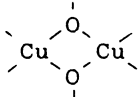


Fig. 10. Structure of  $\text{BaCu}(\text{maae}) \cdot 7\text{H}_2\text{O}$  (**15**). Two of the six water molecules in this figure are weakly bonded to the neighboring barium atom so that  $(\text{H}_2\text{O})_2\{\text{Ba}(\text{H}_2\text{O})_4\text{Cu}(\text{maae})\}_2$  and four crystal water molecules form a unit cell.

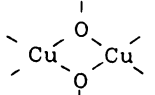
ethyl)malonamide) (**15**) with a  skeleton

(Fig. 10)<sup>26)</sup> show no distinct absorption band in the near-

ultraviolet region. Hence, it is clear that 

skeleton is deeply associated with the appearance of the CT band in the near-ultraviolet region.

The structural comparison of the dialkoxo-bridged binuclear copper(II) complexes, **3a**, **7a**, **10**, **11b**, and **12a** (Table 5), with the complexes **13**—**15** which have no

 skeleton (Table 7) has revealed that the

most conspicuous structural difference between the above two complex groups is the separation of the two bridging oxygens, but not the planarity of the bridging skeleton, though this has been often correlated to magnetic and spectral properties by many authors:<sup>2-8)</sup> The O—O distances of the former group (Table 5) are significantly shorter (ca. 0.4 Å) than those of the latter group (Table 7), whereas no definite difference can be observed in  $\rho$  values, e.g.,  $\rho$  (**12a**)=341° which is nearly equal to the values 340° (**14**) and 342° (**13**).

The deprotonated alcoholic oxygen in the binuclear skeleton has a minus charge,  $e^-$ . Hence, an electrostatic repulsion between the bridging oxygens should elevate the energy of the oxygen's nonbonding orbital when the two oxygens is sufficiently approached by each other. The red-shift of the CT band due to the formation of dialkoxo-bridging may be explained in terms of an energy increase of the nonbonding orbital caused by shortening of the O—O distance. Based on the point charge model<sup>27)</sup> (see Appendix), the repulsion energy  $E$  between two monovalent anions with the separation of  $R$  may be estimated by a very simple function of  $R$ :

$$E = e^2 / R.$$

If we assume  $R_1=2.4$  Å for the O—O distance of the dialkoxo-bridged binuclear copper(II) complexes and  $R_2=2.8$  Å for the O—O (cis position) distance in the cases of **13**—**15**, the difference in repulsion energy between the two anionic pairs  $\Delta E$  is evaluated as follows.

Table 7. Structural Parameters for **13**—**15**

| Complex  | $\rho^a)$<br>°    | O—O<br>Å           | Ref. |
|--|-------------------|--------------------|------|
| [Cu(eta)(Heta)] <sub>2</sub> (NO <sub>3</sub> ) <sub>2</sub> ( <b>13</b> )                   | 342 <sup>b)</sup> | 2.80 <sup>b)</sup> | 25   |
| [Cu(mep)(Hmep)(H <sub>2</sub> O)] <sub>2</sub> (NO <sub>3</sub> ) <sub>2</sub> ( <b>14</b> ) | 340 <sup>b)</sup> | 2.86               | 25   |
| BaCu(maae)·7H <sub>2</sub> O ( <b>15</b> )   | 336 <sup>b)</sup> | 2.79               | 26   |

a) Sum of the bond angles around the alkoxo oxygen;  $\angle\text{Cu—O—C} + \angle\text{Cu—O—H} + \angle\text{C—O—H}$  for **13** and **14**, and  $\angle\text{Cu—O—Ba} + \angle\text{Cu—O—C} + \angle\text{C—O—Ba}$  for **15**. b) Mean value.

$$\Delta E = e^2 \left( \frac{1}{R_1} - \frac{1}{R_2} \right) = e^2 \left( \frac{1}{2.4 \text{ Å}} - \frac{1}{2.8 \text{ Å}} \right) = 6.9 \times 10^3 \text{ cm}^{-1}$$

This value enables us to give the interpretation that the CT band is red-shifted by a few thousand wavenumbers owing to the electrostatic repulsion and may be observed in the near-ultraviolet region.

As for the point (ii), the simple point-charge model is not effective because the O—O distance of **12a** is comparable to those of **3a**, **7a**, **10**, and **11b** (0—0.12 Å longer). The access of perchlorate oxygens to the bridging oxygens could not cause a significant effect on the oxygen nonbonding orbital energy, since all the oxygen atoms of the perchlorate ions are sufficiently apart from the bridging oxygen atoms (the nearest 3.264(9) Å (O1—O3<sup>i</sup>)). Axial coordination of perchlorate ion is also not likely to be the major factor for the red-shift, since even an axially ligated complex, such as **3a**, shows the CT band at the frequency higher than  $25 \times 10^3 \text{ cm}^{-1}$ . Moreover, **12a** does not show any shift of the d—d band (cf. Table 6), and hence the interaction between the copper  $d_{\pi}$ -orbital and the oxygen nonbonding orbital may not be so considerable because the interaction should affect the d—d transition energy.

In view of the above consideration, we propose a more sophisticated interpretation based on the selection rule for the complicated phenomenon as a possible one. The orbitals participating in the CT transition can be expressed as the following wave functions,

$$\begin{aligned} \Psi_I &= p_{\pi^1} + p_{\pi^2} & \Psi_{II} &= p_{\pi^1} - p_{\pi^2} \\ \Psi_{III} &= d_{\sigma^1} + d_{\sigma^2} & \Psi_{IV} &= d_{\sigma^1} - d_{\sigma^2} \end{aligned}$$

where  $p_{\pi^1}$ ,  $p_{\pi^2}$ ,  $d_{\sigma^1}$ , and  $d_{\sigma^2}$  denote nonbonding oxygen

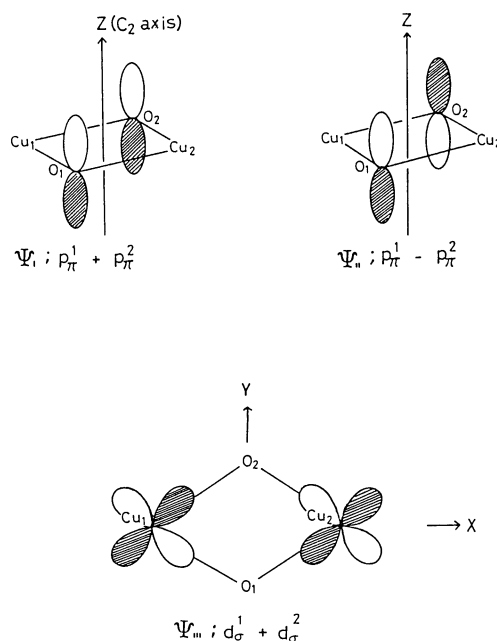
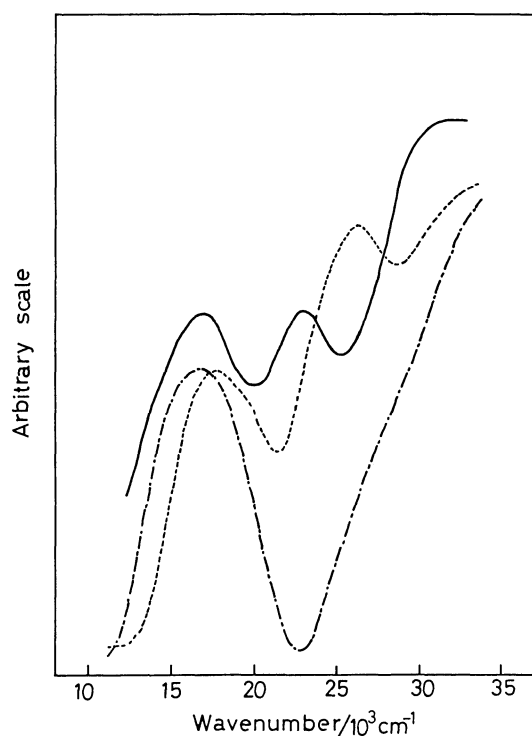


Fig. 11. Schematic representations of the orbitals participating in the CT transition,  $\Psi_I = p_{\pi^1} + p_{\pi^2}$ ,  $\Psi_{II} = p_{\pi^1} - p_{\pi^2}$ ,  $\Psi_{III} = d_{\sigma^1} + d_{\sigma^2}$ .



Table 8. Irreducible Representations of  $\Psi_I$ ,  $\Psi_{II}$ , and  $\Psi_{III}$  and the Direct Products between the Orbitals under Various Symmetries

|   | $D_{2h}$ | $C_{2h}$ | $C_2$ |
|---|----------|----------|-------|
| $\Psi_I$                                  | $b_{1u}$ | $a_u$    | $a$   |
| $\Psi_{II}$                               | $b_{3g}$ | $b_g$    | $b$   |
| $\Psi_{III}$                              | $b_{1g}$ | $a_g$    | $a$   |
| $r \begin{cases} X \\ Y \\ Z \end{cases}$ | $b_{3u}$ | $b_u$    | $b$   |
|   | $b_{2u}$ | $b_u$    | $b$   |
|   | $b_{1u}$ | $a_u$    | $a$   |
| $\Psi_I \times \Psi_{III}$                | $a_{1u}$ | $a_u$    | $a$   |
| $\Psi_{II} \times \Psi_{III}$             | $b_{2g}$ | $b_g$    | $b$   |

Fig. 12. Reflectance spectra of  $\text{Cu}(\text{Me-3-3})\text{ClO}_4$  (**12a**) (—),  $\text{Cu}(\text{n-Bu-3-2})\text{ClO}_4$  (**10**) (---), and  $\text{Cu}(\text{H-3-2})\text{ClO}_4 \cdot 1/8 \text{ MeCN}$  (**6a**) (— · —).

p- and vacant copper d-orbitals, respectively, and the superiors represent the respective atoms (cf. Fig. 11).<sup>28)</sup> Taking into account the theoretical results for the anti-ferromagnetically coupled dicopper system,<sup>3a,c)</sup>  $\Psi_{III}$  is energetically higher than  $\Psi_{IV}$ . Hence, the possible CT band is the transition to  $\Psi_{III}$  from  $\Psi_I$  or  $\Psi_{II}$ .<sup>29)</sup> Irreducible representations of  $\Psi_I$ ,  $\Psi_{II}$ , and  $\Psi_{III}$  and the direct products of them are shown in Table 8. In  $C_2$  symmetry, both  $\Psi_I \rightarrow \Psi_{III}$  and  $\Psi_{II} \rightarrow \Psi_{III}$  electronic dipole transitions are allowed, but in  $D_{2h}$  symmetry no transition is allowed. In  $C_{2h}$  symmetry, only the  $\Psi_I \rightarrow \Psi_{III}$  transition is allowed. The complex cations of **7a**, **10**, and **11b** have a centrosymmetry and a quasi symmetry plane including the  $\text{Cu}_2\text{O}_2$  core in their molecules, hence the complexes can be approximated by  $C_{2h}$  symmetry. Thus, the observed CT band for the complexes can be

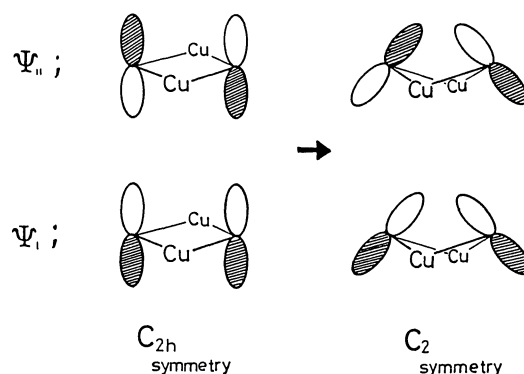
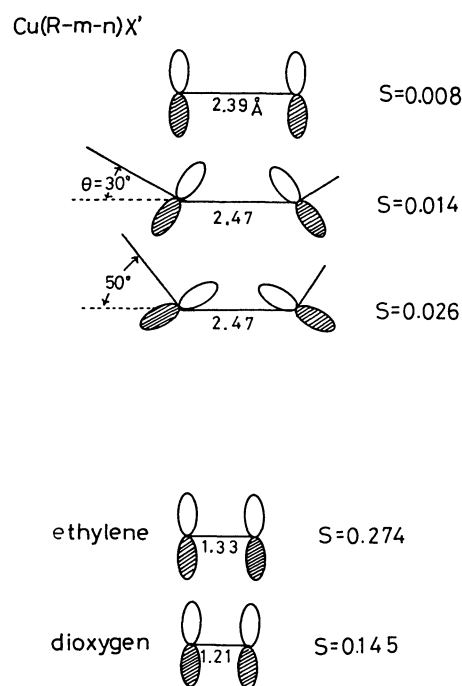
Fig. 13. Orbitals  $\Psi_I$  and  $\Psi_{II}$  under  $C_{2h}$  and  $C_2$  symmetries.

Fig. 14. Results of calculations of the overlap integrals.

assigned to the  $\Psi_I \rightarrow \Psi_{III}$  transition. The reflectance spectrum of **12a** is shown in Fig. 12, together with those of **6a** and **10**. It is clearly seen that the frequency and intensity of the CT band maximum of **12a** are both lower than those of **10**. The frequency of the band maximum of **12a** is lower than that of **10** by ca.  $3 \times 10^3 \text{ cm}^{-1}$ . The intensity of the CT band of **12a** is comparable to that of its d-d transition band while, in the case of **10**, the intensity of the CT band is relatively higher than that of the d-d band. As mentioned in the previous section, the most noticeable feature of **12a** is a bent structure with a roof-shaped  $\text{Cu}_2\text{O}_2$  ring and a small dihedral angle ( $D=158.2^\circ$ ) between two  $\text{CuO}_2$  planes. Accordingly, the symmetry of the complex cation is regarded as  $C_2$  symmetry, which should allow both transitions  $\Psi_I \rightarrow \Psi_{III}$  and  $\Psi_{II} \rightarrow \Psi_{III}$ . In the CD spec-

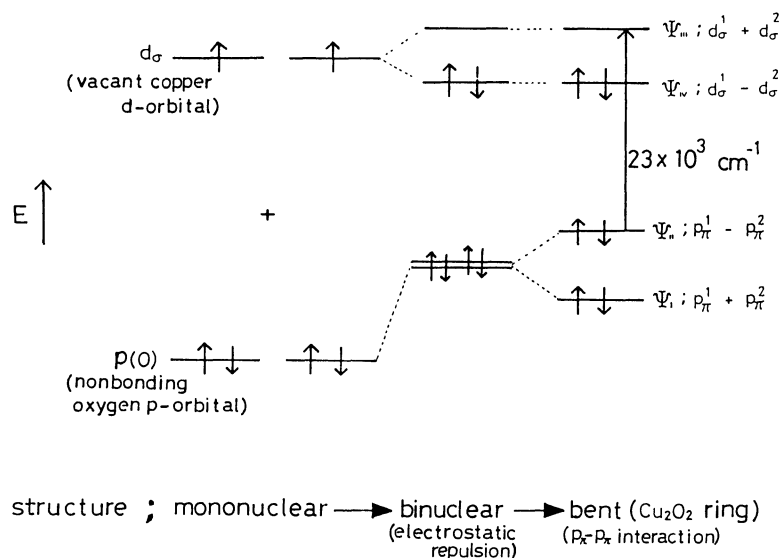


Fig. 15. Schematic illustration for the appearance of the CT band at  $23 \times 10^3 \text{ cm}^{-1}$ .

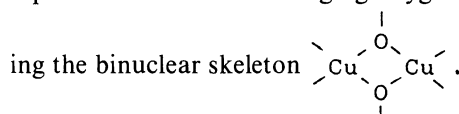
trum, corresponding two bands (at  $28.2$  and  $24.8 \times 10^3 \text{ cm}^{-1}$ ) have been observed for a dialkoxo-bridged binuclear copper(II) complex with optically active *N*-(3-hydroxypropyl)-(-)-1,2-propanediamine.<sup>8)</sup>

In order to discuss the effect of the lowering of symmetry from  $C_{2h}$  to  $C_2$ , i.e., from planer to bent structure, on the energies of  $\Psi_I$  and  $\Psi_{II}$ , the variation of the nonbonding p-orbitals is schematically illustrated in Fig. 13. The transformation  $C_{2h} \rightarrow C_2$  causes the increase of an interaction between two nonbonding p-orbitals and this leads to the increase in energy separation of the  $\Psi_I$  and  $\Psi_{II}$  orbitals since  $\Psi_I$  and  $\Psi_{II}$  have bonding and antibonding characters, respectively. The CT band at ca.  $23 \times 10^3 \text{ cm}^{-1}$  observed in **12a** and **12b** is assigned to the  $\Psi_{II} \rightarrow \Psi_{III}$  transition which is forbidden under  $C_{2h}$  symmetry. The transition is now allowed by the symmetry degradation,  $C_{2h} \rightarrow C_2$ . The low intensity of the CT bands of **12a** and **12b** may be due to this fact. The  $\Psi_I \rightarrow \Psi_{III}$  transition which is expected to appear at a higher frequency is probably hidden by the intense CT band around  $31 \times 10^3 \text{ cm}^{-1}$  attributable to a  $\sigma(\text{O}) \rightarrow d\sigma(\text{Cu})$  transition.

The magnitude of the interaction between the two nonbonding p-orbitals was estimated by calculating their overlap integrals according to Mulliken's treatment.<sup>30)</sup> The results illustrated in Fig. 14 indicate that the overlap integral  $S=0.026$  at  $\theta=50^\circ$ ,  $\theta=50.3^\circ$  (mean value) for **12a**, is about 1/10 of those of ethylene or dioxygen molecules whose  $\pi-\pi^*$  transition energies are of the order ca.  $10^4 \text{ cm}^{-1}$ .<sup>31,32)</sup> Consequently, it is plausible that the interaction between two nonbonding p-orbitals is large enough to cause the energy shift of a few thousand wavenumbers to lower energy as observed for **12a**. Schematic illustration for the appearance of the CT band at a very low frequency  $23 \times 10^3 \text{ cm}^{-1}$  is shown in Fig. 15.

## Conclusion

The near-ultraviolet absorption bands observed in the type-A dialkoxo-bridged binuclear copper(II) complexes are assigned to the charge transfer (CT) transition from the nonbonding orbital of bridging oxygen to the vacant copper d-orbital, and the appearance of the CT band in the near-ultraviolet region is interpreted in terms of the red-shift of the band due to the electrostatic repulsion between two bridging oxygen atoms on forming the binuclear skeleton



The unusually low frequency (ca.  $23 \times 10^3 \text{ cm}^{-1}$ ) and low intensity of the CT band observed for **12a** and **12b** is interpreted in terms of the increased interaction between the bridging oxygen atoms in the bent structure.

## Appendix

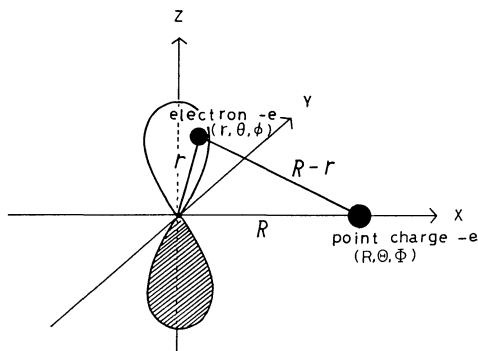
In this calculation it is assumed that the nonbonding orbital of the bridging oxygen atom is of pure p-character. When the potential  $V$  for an electron on a nonbonding orbital of one oxygen atom is generated by the point charge ( $-e$ ) of the other deprotonated alkoxo oxygen, the potential  $V$  is expressed by

$$V = \frac{e^2}{|\mathbf{R} - \mathbf{r}|},$$

where  $\mathbf{R}$  and  $\mathbf{r}$  are vectors defined as shown at the top of the next page (left side). Then, the repulsion energy  $E$  is calculated by the equation

$$E = \langle P_0 | V | P_0 \rangle,$$

where  $P_0 = R_{2,1}(r) Y_{1,0}(\theta, \phi)$ , and  $R_{2,1}$  and  $Y_{1,0}$  denote a radial function and spherical harmonic for  $p_z$  orbital of oxygen atom, respectively.



$e^2/|\mathbf{R}-\mathbf{r}|$  can be expressed in spherical harmonics by using the spherical coordinates  $(r, \theta, \phi)$  and  $(R, \Theta, \Phi)$  for  $\mathbf{r}$  and  $\mathbf{R}$ , respectively. Consequently, the potential  $V$  is represented by the equation

$$V(r, \theta, \phi) = \frac{e^2}{R} \sum_{k=0}^{\infty} \frac{4\pi}{2k+1} \left(\frac{r}{R}\right)^k \sum_{m=-k}^k Y_{km}(\theta, \phi) Y_{km}^*(\Theta, \Phi).$$

In the case of  $(\Theta, \Phi) = (\pi/2, 0)$ , the equation can be reduced to:

$$V(r, \theta, \phi) = \frac{e^2}{R} - \frac{e^2 r^2}{2R^3} C_0^{(2)}(\theta, \phi),$$

$$C_0^{(2)}(\theta, \phi) = \sqrt{\frac{4\pi}{5}} Y_{20}(\theta, \phi).$$

Finally, the repulsion energy between bridging oxygen atoms is obtained by Eq. 2,

$$\begin{aligned} E &= \langle p_0 | V | p_0 \rangle \\ &= \frac{e^2}{R} \left( 1 - \frac{1}{5} \frac{\bar{r}^2}{R^2} \right), \end{aligned} \quad (2)$$

where  $\bar{r}^2 = \langle R_{2,1} | r^2 | R_{2,1} \rangle$  represents the integral for the radial part.

The integral calculation of  $\langle R_{2,1} | r^2 | R_{2,1} \rangle$  gives  $\bar{r}^2 = 15a_0^2/32$  ( $a_0$  is Bohr radius (0.529 Å)). If  $R = 2.4$  Å is assumed, the second term in the parenthesis of Eq. 2 is negligible;

$$\begin{aligned} \frac{1}{5} \left( \frac{\bar{r}^2}{R^2} \right) &= \frac{1}{5} \cdot \frac{15}{32} \left( \frac{0.529}{2.4} \right)^2 \\ &= 0.0046 \ll 1 \end{aligned}$$

Accordingly, the repulsion energy may be simply estimated with  $e^2/R$ .

## References

- 1) A part of dissertation of M. Handa for the degree of Doctor of Science, Kyushu University, 1990.
- 2) e.g., a) L. Merz and W. Haase, *J. Chem. Soc., Dalton Trans.*, **1980**, 875; b) L. Walz, H. Paulus, and W. Haase, *ibid.*, **1985**, 913; c) L. Walz and W. Haase, *ibid.*, **1985**, 1243; d) K. Nieminen, *Ann. Acad. Sci. Fenn., Ser. A2*, **197**, 1 (1983); (e) M. Mikuriya, K. Toriumi, T. Ito, and S. Kida, *Inorg. Chem.*, **24**, 629 (1985).
- 3) e.g., a) P. J. Hay, J. C. Thibault, and R. Hoffmann, *J. Am. Chem. Soc.*, **97**, 4884 (1975); b) H. Astheimer and W. Haase, *J. Chem. Phys.*, **85**, 1427 (1986); c) M. Handa, N. Koga, and S. Kida, *Bull. Chem. Soc. Jpn.*, **61**, 3853 (1988).
- 4) E. Uhlig and K. Staiger, *Z. Anorg. Allg. Chem.*, **346**, 21 (1966); **360**, 39 (1968).
- 5) Y. Nishida and S. Kida, *J. Inorg. Nucl. Chem.*, **38**, 451 (1976).
- 6) N. Matsumoto, I. Ueda, Y. Nishida, and S. Kida, *Bull. Chem. Soc. Jpn.*, **49**, 1308 (1976).
- 7) Y. Ishimura, Y. Nonaka, Y. Nishida, and S. Kida, *Bull. Chem. Soc. Jpn.*, **46**, 3728 (1973).
- 8) S. Kida, Y. Nishida, and M. Sakamoto, *Bull. Chem. Soc. Jpn.*, **46**, 2428 (1973).
- 9) Y. Nishida and S. Kida, *Chem. Lett.*, **1974**, 339; N. Matsumoto, Y. Nishida, S. Kida, and I. Ueda, *Bull. Chem. Soc. Jpn.*, **49**, 117 (1976).
- 10) Y. Nishida, F. Numata, and S. Kida, *Inorg. Chim. Acta*, **11**, 189 (1974).
- 11) M. Mikuriya, T. Toki, I. Murase, H. Ōkawa, and S. Kida, *Synth. React. Inorg. Met.-Org. Chem.*, **15**, 965 (1985).
- 12) M. Mikuriya, M. Nakamura, H. Ōkawa, and S. Kida, *Chem. Lett.*, **1982**, 839; M. Nakamura, M. Mikuriya, H. Ōkawa, and S. Kida, *Bull. Chem. Soc. Jpn.*, **54**, 1825 (1981).
- 13) L. Banci and A. Dei, *Inorg. Chim. Acta*, **39**, 35 (1980).
- 14) R. N. Keller and L. J. Edwards, *J. Am. Chem. Soc.*, **74**, 215 (1952).
- 15) N. F. Curtis, *J. Chem. Soc.*, **1961**, 3147.
- 16) "International Tables for X-Ray Crystallography," Kynoch Press, Birmingham (1974), Vol. 4.
- 17) T. Sakurai and K. Kobayashi, *Rikagaku Kenkyusho Hokoku*, **55**, 69 (1979).
- 18) S. Kawano, *Rep. Comput. Cent. Kyushu Univ.*, **13**, 39 (1980).
- 19) P. Main, S. E. Hull, L. Lessinger, G. Germain, J.-P. Declercq, and M. M. Woolfson, "MULTAN 78, A System of Computer Programs for the Automatic Solution of Crystal Structures from X-Ray Diffraction Data," University of York (1978).
- 20) C. K. Johnson, "Report No. 3794," Oak Ridge National Laboratory, Oak Ridge, Tennessee (1965).
- 21) A. C. Villa, L. Coghi, A. G. Manfredotti, and C. Guastini, *Cryst. Struct. Commun.*, **3**, 543 (1974).
- 22) N. Matsumoto, S. Kida, and I. Ueda, *J. Coord. Chem.*, **9**, 133 (1979).
- 23) See Refs. 2d and 3c, and references therein.
- 24) e.g., B. J. Hathaway and A. A. G. Tomlinson, *Coord. Chem. Rev.*, **5**, 1 (1970); B. J. Hathaway and D. E. Billing, *ibid.*, **5**, 143 (1970); B. J. Hathaway, *Struct. Bonding (Berlin)*, **57**, 55 (1984); A. B. P. Lever, "Inorganic Electronic Spectroscopy," Elsevier, Amsterdam (1968), Chap. 9.
- 25) S. Kida, *Nippon Kagaku Zasshi*, **85**, 428 (1964); J. A. Bertrand, E. Fujita, and D. G. VanDerveer, *Inorg. Chem.*, **19**, 2022 (1980); E. Fujita, Ph. D. Thesis, Georgia Institute of Technology, 1976.
- 26) T. Toki, M. Mikuriya, H. Ōkawa, I. Murase, and S. Kida, *Bull. Chem. Soc. Jpn.*, **57**, 2098 (1984).
- 27) H. L. Schäfer and G. Gliemann, "Basic Principles of Ligand Field Theory," Wiley-Interscience, London-New York-Sydney-Toronto (1969); H. Kamimura, S. Sugano, and T. Tanabe, "Ligand Field Theory and Its Applications," Syokabo, Tokyo (1969).
- 28) The magnetic coupling occurs through the bridging oxygen's p- or s-orbitals combined with the copper d-orbital. Here, however, the orbitals  $\Psi_I$  and  $\Psi_{II}$  are simply described by the p-orbitals, and  $\Psi_{III}$  and  $\Psi_{IV}$ , by the d-orbitals, because we do not intend to discuss the magnetic coupling.
- 29) This assignment has been experimentally confirmed by the fact that the CT band intensity increases with lowering of

temperature in the dialkoxo-bridged binuclear copper(II) complex  $[\text{Cu}_2(\text{pn-prol})_2](\text{ClO}_4)_2$ ,  $\text{H}(\text{pn-prol})=N$ -(3-hydroxypropyl)-(-)1,2-propanediamine (cf. Ref. 8).

30) R. S. Mulliken, C. A. Rieke, D. Orloff, and H. Orloff, *J. Chem. Phys.*, **17**, 1248 (1949).

31) P. G. Wilkinson and R. S. Mulliken, *J. Chem. Phys.*,

**23**, 1895 (1955); A. J. Merer and R. S. Mulliken, *Chem. Rev.*, **69**, 639 (1969).

32) e.g., E. A. V. Ebsworth, D. W. H. Rankin, and S. Cradock, "Structural Methods in Inorganic Chemistry," Blackwell Scientific Publications, Oxford-London-Edinburgh-Boston-Palo Alto-Melbourne (1987), Chap. 6.

---